Li *et al.*
Journal of Engineering and Applied Science (2022) 69:89
https://doi.org/10.1186/s44147-022-00140-1

Journal of Engineering and Applied Science

RESEARCH Open Access

Reproduction method of time-domain load of construction machinery internal combustion engine

Zhijie Li[1], Yonglai Wang[1*], Chaoqin Liu[2], Weicheng Kong[2] and Cuicui Chen[1]

*Correspondence:
wangyonglai@weichai.com

[1] State Key Laboratory of Engine Reliability, Weifang, China
[2] School of Mechanical and Aerospace Engineering, Jilin University, Changchun, China

Abstract

Bench test has been proved to be an effective method in the field of fatigue life prediction and reliability design for construction machinery internal combustion engine (CMICE), and the reasonable load reproduction is a promising supplement to the experimental data. To reproduce the load reasonably and eliminate the limitation that traditional peak over threshold (POT) extrapolation only focuses on extreme load, a method to reproduce the time-domain load of CMICE is proposed in this paper. Here, the extreme load is reproduced with POT model, where the upper and lower thresholds are selected through the mean excess function graph, while the intermediate load is reproduced by fitting the Gaussian mixed distribution. The load before and after reproduction is compared with the results of through-level counting and pseudo-damage calculation, which verifies the rationality of the proposed time-domain load reproduction method.

Keywords: CMICE, POT model, Threshold selection, Time-domain load reproduction

Introduction

Nowadays, the requirements for the reliability of the internal combustion engine (ICE) in the industry of engineering machinery are gradually increasing. The reliability research of the ICE involves two aspects: the reliability of the whole machine and the reliability of the parts. Regarding the reliability evaluation of the whole machine, the mainstream research contents include the monitoring of the health status of the ICE and the compilation of the load spectrum of the whole machine [1–3]. The reliability research of the parts mainly focuses on the key components such as the crankshaft, connecting rod, piston, and cylinder head. Finite element analysis of key positions and fatigue life evaluation of components based on the S-N curve are mainly adopted [4–7]. In addition, the capacity to maintain ICE's toxic emission reliably is also a very important aspect of its reliability research, especially when ICE works in harsh environments such as high altitude, cold and high temperature. As far as the whole engine, there are studies on the reliability test, evaluation and optimization of ICE in the plateau area [8–11]. In terms of pars, there are studies on the reliability evaluation and prediction of cylinder liner

as well as cylinder head considering both thermal boundary conditions and mechanical loads [12, 13], and there are also studies on the condition monitoring of key components such as cylinder liner and piston ring under harsh conditions such as high temperature, high pressure, and heavy load [14, 15].

Both the reliability of the whole machine and the reliability of the parts need the study of internal combustion engine load. It is an essential step to reproduce the working load of internal combustion engine for bench test or fatigue simulation calculation. In the process of compiling load spectrum of CMICE, reasonable load reproduction is very important. Common load reproduction methods include rain flow matrix extrapolation, parameter method extrapolation, mileage and quantile extrapolation, and timely extra-territorial extrapolation [16–18]. When reproducing the time-domain load, the extreme load is often reproduced. The commonly used extreme extrapolation models include POT model [19–21], block maximum method [22–24], method of independent storms [25, 26], and so on. Among them, POT model has received wide attention for its low demand for data volume and great reflection of data characteristics.

In the study of load reproduction based on POT model, threshold selection is a very important issue. The threshold can be selected based on the empirical average excess function, but it is susceptible to subjectivity to a large extent in the process of observing the scatter plot of the empirical average excess function. The rationality of the threshold selection can be evaluated by means of square error of the shape parameters of the generalized Pareto distribution (GPD) obeyed by the extreme load [27]. Liang et al. [28] proposed an automatic threshold selection method based on the extrapolation of indigenous wave height characteristics, which simplified the threshold selection process and reduced the subjectivity in the selection process. To improve the credibility of threshold selection, Wang et al. [29, 30] proposed the automatic selection method of threshold based on bootstrapping technology and multi-criteria decision-making technology. Yang et al. [31] proposed the selection method of POT model threshold by improving the traditional mean excess function, which ensures the fitting accuracy and avoids the errors caused by subjective factors.

At present, most studies tend to pay more attention to the extreme load, while under the action of random load, the intermediate load has an impact on the fatigue life that cannot be ignored, which is also of engineering significance to reproduce the low strength load. There are related works on the reconstruction and reproduction of the intermediate load between the thresholds. Liu [32] and Wang [33] reconstructed the load between the upper and lower thresholds based on the traditional POT extrapolation.

Since POT extrapolation focuses on the extreme load in the timing signal but does not process the intermediate load between the upper and lower thresholds, it will lead to the lack of diversity and randomness of the test data. In this paper, a new method of time-domain load reproduction of CMICE is proposed to make the reproduced time-domain load more diverse, random and close to the real situation on the premise of conforming to the original data characteristics. In addition, the exceedance mean function graph method is used when selecting the thresholds to avoid the large error caused by subjective judgment. Firstly, the collected ICE data are preprocessed, and outliers in the data are eliminated. Then, the gradient value of the ICE speed data is calculated. The user conditions—the shutdown, idle, and three operating conditions—are divided by

the range of the average speed between the adjacent two large gradients. Based on the POT model, the upper and lower extreme values of the data in the working condition are extrapolated, and the intermediate loads between the upper and lower thresholds are reproduced based on the Gaussian mixed distribution. Finally, the load data before and after reproduction are counted and the pseudo-damage of ICE is calculated. The rationality of the proposed time-domain load reproduction method is verified by comparing the above results. The diagram of proposed method for load reproduction is shown in Fig. 1.

Methods

Data preprocessing

Elimination of outlier

The torque and speed signals of the excavator ICE are collected through Controller Area Network (CAN) bus. Working in the poor environment and complex conditions leads to the instantaneous mutation of the load data obtained by the test due to the channel noise and external environment interference, namely, the outliers in the data, which are often far greater than or far less than the normal operating data value. These values will have a great impact on the load reproduction of the ICE and the calculation results of the pseudo damage. Therefore, before the load reproduction, the ICE data should be preprocessed to eliminate these abnormal data.

At present, the amplitude threshold method, gradient threshold method, and boxplot method [34] are the most commonly used methods in engineering to eliminate singular values. The amplitude threshold method is suitable for the singular value exceeding the

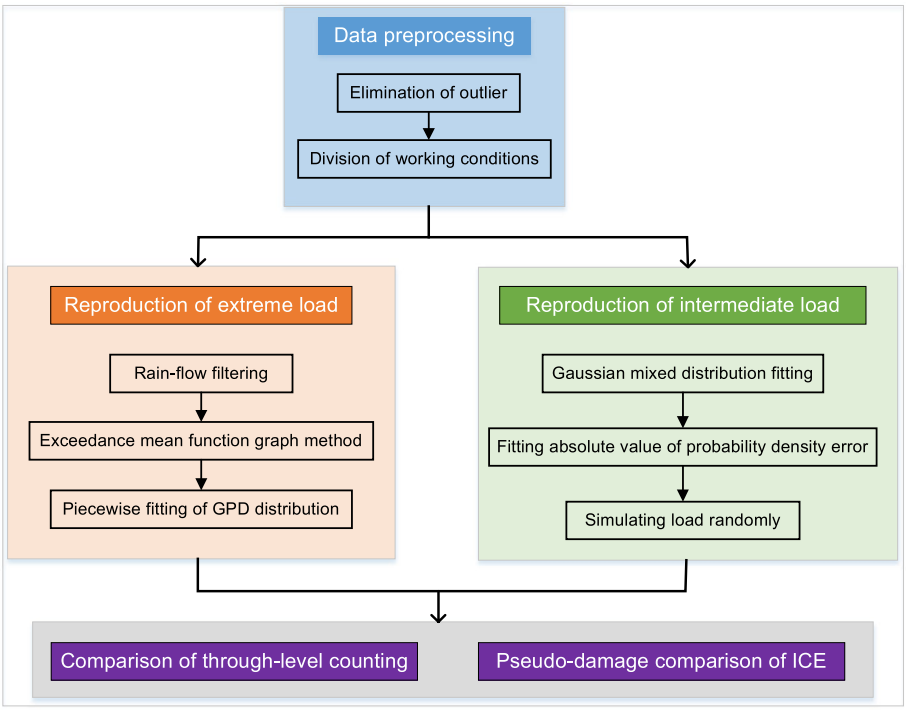

Fig. 1 The diagram of proposed method for load reproduction

maximum or minimum load value, which is used to eliminate the singular load exceeding the speed and torque limit in this paper.

Since the speed and torque data of ICEs collected by CAN bus are real-time corresponding, the speed and torque data after the elimination of abnormal values also need to be corresponding in the time-domain. In view of this situation, when the rotational speed and torque values at a certain time both exceed their respective limit load values, the rotational speed and torque values at that time are both eliminated. If only one load at a certain time is a singular value, for example, the torque value exceeds its limit load value, and the rotational speed value belongs to the normal value, then the rotational speed data at that time are retained, and the corresponding torque value is taken as the limit load value. The diagram of the amplitude threshold method to eliminate the singular value of ICE data is shown in Fig. 2.

Division of working conditions

The speed and torque time series of the ICE are shown in Fig. 3. To ensure the stability of the load, working conditions are divided based on average speed. By observing the change of data, it can be seen that the range of speed fluctuation is 0–1800 rpm. When the speed is 0–900 rpm, the torque is very small and almost constant, which can be considered the shutdown stage; when the rotational speed is 900–1400 rpm, the rotational speed is almost constant and the torque is almost 0, so it can be regarded as the idle stage; when the rotational speed is 1400–1700 rpm, it is the normal operating stage of the excavator, and then the operating conditions are further divided based on the gradient of rotational speed.

Speed gradient refers to the change value between two adjacent speed data in unit time. The calculation formula is as follows:

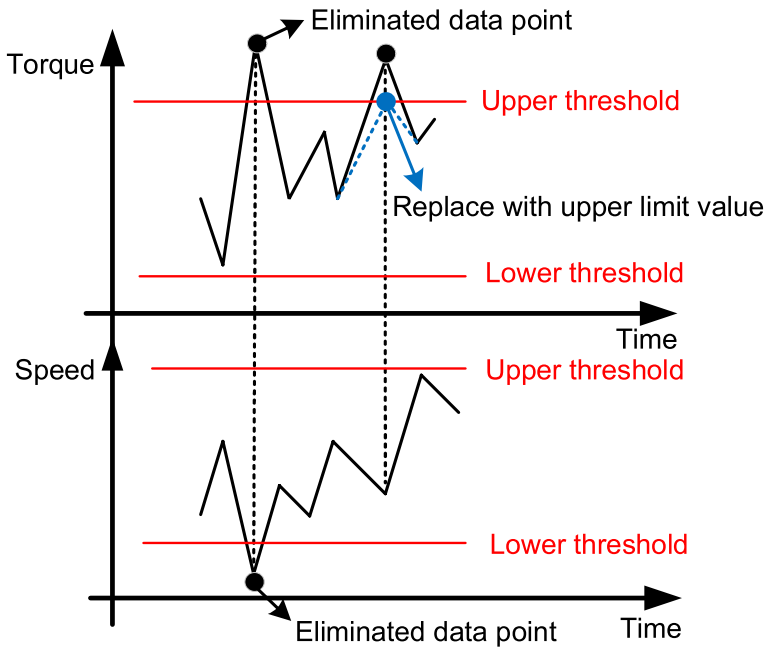

Fig. 2 Diagram of the amplitude threshold method

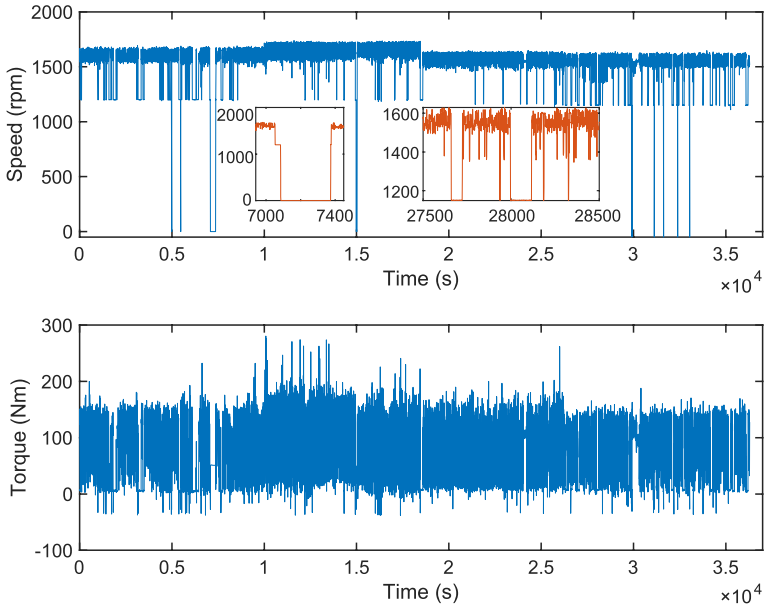

Fig. 3 Time series of ICE speed and torque

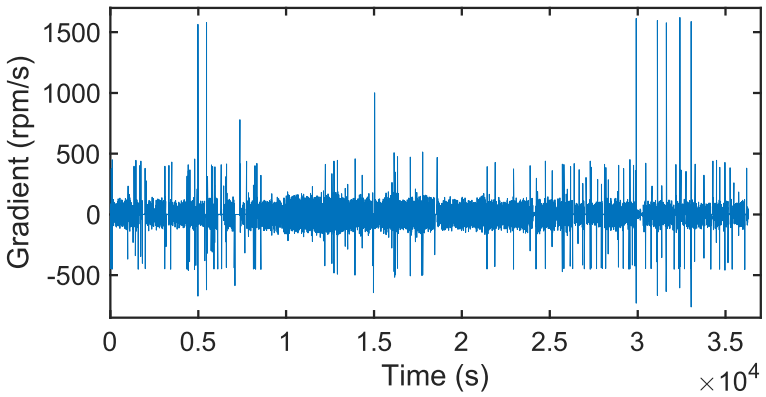

Fig. 4 Speed gradient diagram of ICE

$$\text{Gradient} = \frac{N_{i+1} - N_i}{T_{i+1} - T_i} \tag{1}$$

where T_i is the moment i, N_i is the speed value of moment i; T_{i+1} is the moment $i+1$, and N_{i+1} represent the speed value of moment $i+1$.

The gradient change of engine speed is shown in Fig. 4. It can be seen from the speed gradient diagram that the large gradient is concentrated above 200 rpm/s and below − 200 rpm/s, so the gradient less than – 200 rpm/s and greater than 200 rpm/s is extracted and marked as a large gradient, and the time points of the large gradient are marked for further division of operating conditions.

The working conditions are divided based on the average speed data between two adjacent large gradients. From the above analysis, it can be seen that the torque is almost 0 when the average rotational speed is 0–900 rpm, which can be regarded as the shutdown stage. When the average speed is 900–1400 rpm, the torque is almost constant, which

Table 1 Number of data points and time ratio of each working condition

Working condition	Average mean of speed rpm	Number of data	Time proportion
Shutdown stage	0–900	379	1.04%
Idle stage	900–1400	3625	9.99%
Operating stage	1400–1500	8001	22.05%
	1500–1600	5847	16.11%
	1600–1700	18,439	50.81%
Total		36,291	100.00%

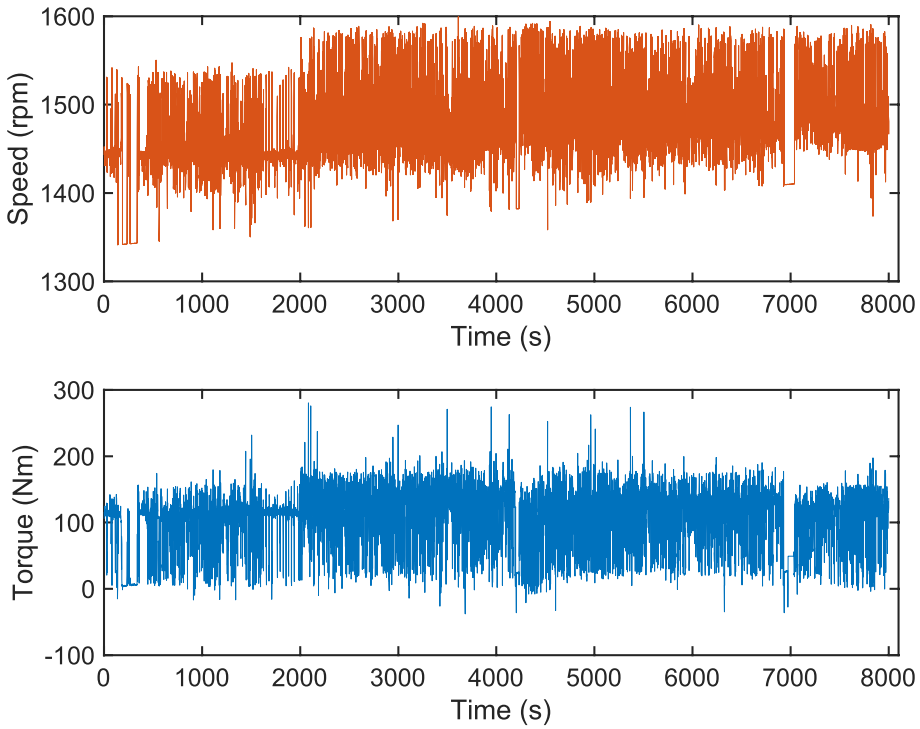

Fig. 5 Time series of ICE speed and torque when the average speed is 1400–1500 rpm

can be regarded as the idle stage; the average speed of 1400–1500 rpm, 1500–1600 rpm, and 1600–1700 rpm can be regarded as different operating stages. The number and time proportion of data points under each working condition are shown in Table 1.

Since the shutdown condition does not cause damage to the ICE, the shutdown condition load spectrum of the ICE is no longer prepared. Idle speed condition can be regarded as a condition of constant speed and almost zero torque value. According to this characteristic and the time proportion of the idle speed condition, the idle speed condition can be directly loaded on the bench, so the load spectrum of the idle speed condition will not be compiled. In this paper, the ICE load is reproduced by taking the operating condition of the average speed at 1400–1500 rpm as an example. It can be seen from Fig. 5 that the speed value in this operation stage fluctuates around an average value in a small range. Generally, the average speed value of the operation stage can be loaded in the bench test, and speed load reproduction is not required. Time series of

ICE speed and torque corresponding to the average speed of 1400–1500 rpm is shown in Fig. 5.

Reproduction of extreme load

The torque time series shown in Fig. 5 is collected by the same driver working on the same material. However, when different drivers work on different materials, the torque extreme load data will vary greatly. In order to fully consider the diversity of working conditions, the maximum and minimum values of torque are reconstructed and reproduced simultaneously, the extreme torque load of excavator ICE is reproduced based on POT model in this paper.

GPD

When the POT model is used to reproduce the extreme load, not all the sample data contain extreme information. The generalized Pareto distribution can be used to fit the tail distribution (upper tail and lower tail) and to describe the distribution characteristics of samples exceeding a certain threshold. The expression of POT Pareto model is as follows:

$$G(x,\sigma,\xi)=\begin{cases}1-\left(1+\xi\frac{x-u}{\sigma}\right)^{-\frac{1}{\xi}},\xi\neq 0,x>u\\ 1-\exp\left(-\frac{x-u}{\sigma}\right),\xi=0,x>u\end{cases} \tag{2}$$

where σ is the proportional parameter; ξ is the shape parameter; u is the threshold.

The extreme torque load is reproduced by changing the GPD probability. Here, the quantile expression of the GPD function is needed, is as follows.

$$X(G)=\begin{cases}\mu-\frac{\sigma}{\xi}\left[1-(1-G_u)^{-\xi}\right],\xi\neq 0\\ \mu+\sigma[-\log(1-G_u)],\xi=0\end{cases},G_u\in(0,1) \tag{3}$$

Threshold selection

In POT model, threshold selection is a key step. The traditional method is usually based on the graphic method and subjective judgment, which has strong subjectivity and uncertainty. In this paper, the exceedance mean function graph method is used to select the threshold. In order to avoid the large error caused by subjective judgment, each candidate threshold is tested both by chi-square test and KS test. The basic idea of this method is as follows: for a series of alternative thresholds, two criteria (KS test statistics and chi-square test) are needed to calculate the corresponding fitting error, and the comprehensive error is obtained based on the entropy method. Then, the threshold corresponding to the minimum comprehensive error is selected as the optimal threshold.

Before the threshold value of torque data in Fig. 5 is selected, rain-flow filtering is needed to eliminate the small amplitude loads in the sequence load sequence. These small-amplitude loads have little contribution to engine damage, and the amount of data is large, which greatly increases the workload. The peak-valley value points of the data are extracted in the process of rain-flow filtering, which is more convenient to select the threshold. Figure 6 shows the local torque time sequence after rain-flow filtering.

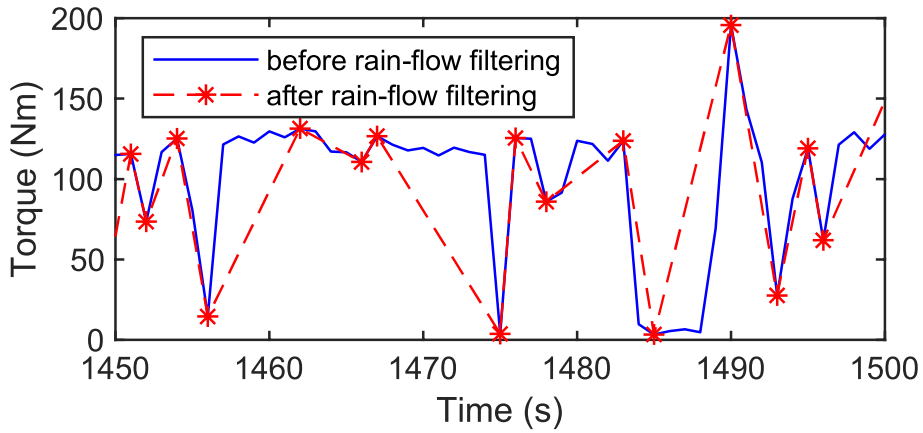

Fig. 6 Torque time series before and after rain filtering

$e(u) = E(X-u|X>u)$ is defined as the mean excess function of X, and Eq. (4) can be obtained based on the properties of GPD.

$$e(u) = E(X-u|X>u) = \frac{\sigma+\xi u}{1-\xi} \tag{4}$$

It can be seen from the above equation that when the shape parameter ξ is a constant, $e(u)$ is a linear function of u. For the measured samples $X_1, X_2, \ldots, X_n$, $e(u)$ is usually unknown, and the mean value function of the sample empirical transcendental quantity is as follows.

$$e_n(u) = \frac{1}{n_u}\sum_{i=1}^{n_u}(X_i - u) \tag{5}$$

According to Eq. (5), the function graph of threshold u and $e_n(u)$ is drawn. If $e_n(u)$ is approximately linear after a certain threshold u, then the optimal threshold is around the threshold u.

Figure 7 is the functional diagram of the threshold u and $e_n(u)$ when the upper threshold of the torque data in Fig. 5 is selected.

In order to reduce the chance of threshold selection, three different time windows $t = 1$, $t = 5$ and $t = 10$ are selected for evaluation, and $t = 5$ represents the extreme value window of 5 s. The changing trend of $e_n(u)$ with the threshold u obtained by different windows is similar. With the increase of the threshold u, the value of $e_n(u)$ increases first and then decreases. The divergence region indicates that the parameters of GPD fitting cannot be estimated, that is, the sample is insufficient to fit the distribution. As can be seen from Fig. 7, when the threshold is between 172 and 176, the change of $e_n(u)$ tends to be linear, so the five values from 172 to 176 are used as candidate thresholds, and the extreme samples are fitted by the GPD function in turn, and the best threshold is determined by chi-square test and KS test (Table 2).

According to the comprehensive judgment index, when the upper threshold of torque load is 175 Nm, the GPD function fitting extreme sample is optimal, so 175 Nm is selected as the upper threshold.

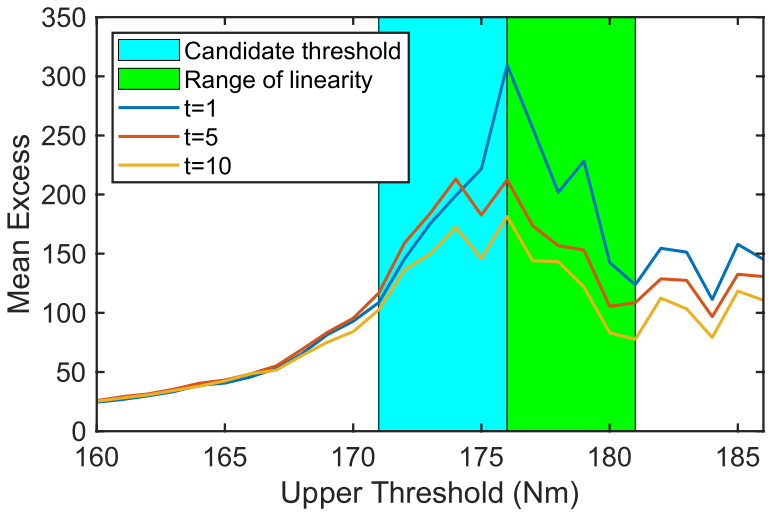

Fig. 7 Graph of the mean excess function

Table 2 Candidate threshold goodness of fit table

Candidate threshold u	KS test	Chi-square test	Shape parameter ξ	Scale parameter σ
172	0.55	0.24	0.43	7.40
173	0.70	0.28	0.48	7.13
174	0.76	0.42	0.51	7.22
175	0.79	0.63	0.54	7.40
176	0.86	0.36	0.62	6.89

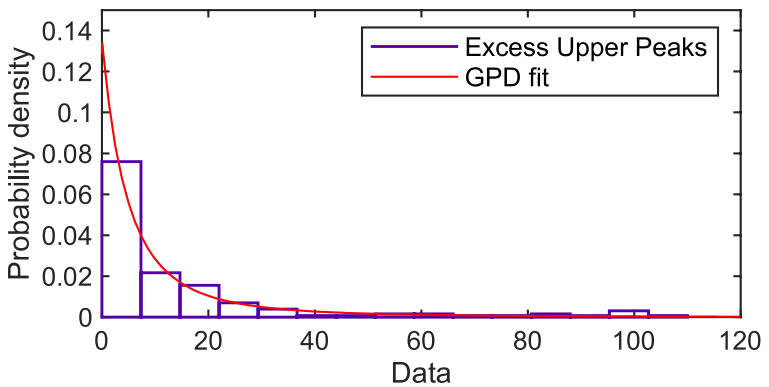

Fig. 8 GPD fitting histogram

When the upper threshold of torque load is 175 Nm, the GPD function is used to fit the extreme value sample. It can be seen from Figs. 8 and 9 that the goodness of fit is high.

The lower threshold of torque load is also selected according to the above steps. The selection process of the lower threshold is omitted here, and the lower threshold is finally determined as 6 Nm.

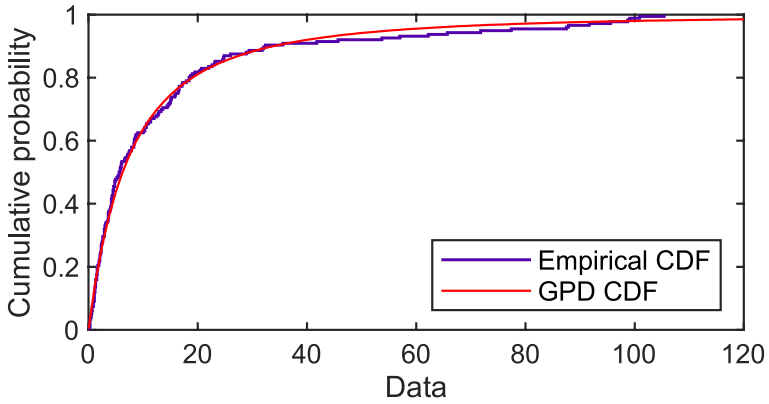

Fig. 9 GPD cumulative probability distribution graph

After obtaining the upper and lower thresholds of torque data, the two thresholds are set as the boundary points of data, where the upper boundary point is set to 175 Nm, and the lower boundary point is set to 6 Nm. After that, the piecewise fitting of GPD distribution is carried out. The segmented expression of paretotails is established, namely the data itself includes the upper tail distribution, interpolation experience distribution and lower tail distribution, fitting as shown in Fig. 10 and Table 3.

After determining the GPD distribution of the upper and lower tails, the torque time series of the ICE is reproduced, and the reproduced results are obtained by randomly adjusting the GPD probability value of the extreme load. The reproduced result of the torque extreme load is shown in Fig. 11.

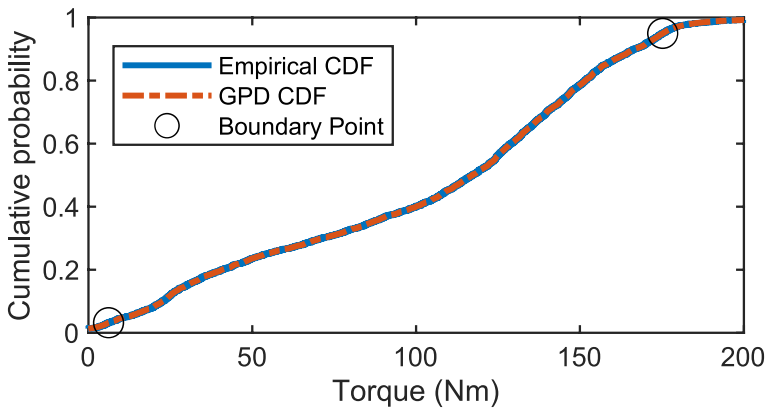

Fig. 10 Paretotails piecewise fitting graph

Table 3 Optimal threshold fitting parameter table

Threshold u	Shape parameter ξ	Scale parameter σ
175 Nm	0.54	7.41
6 Nm	0.32	5.68

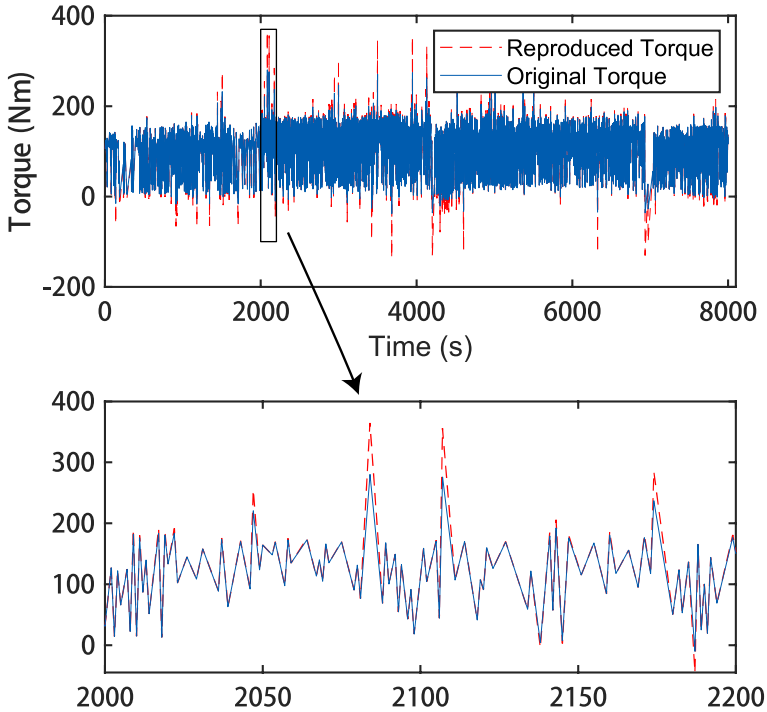

Fig. 11 Comparison of torque extreme value of ICE before and after reproduction

Reproduction of intermediate load

The traditional time-domain load reproduction based on POT model only reproduces the extreme load beyond the upper and lower thresholds, while the intermediate load within the threshold remains unchanged. However, in the actual operation, due to the diversity of external factors such as operating materials and drivers' driving habits, the intermediate load of the ICE will also change under the same working condition. In order to make the load reproduction result more in line with the actual situation, this paper also reproduces the intermediate load within the threshold.

In this paper, the intermediate load is fitted based on the Gaussian mixed distribution, and the probability density error between the actual load and the theoretical distribution is fitted by the normal distribution. The limit error value of the probability density value is calculated by the fitting parameters of the normal distribution, and the intermediate load is predicted in the range of the limit error value. The specific contents are as follows:

(1) The intermediate load within the threshold is fitted with Gaussian mixed distribution, the probability density function expression of Gaussian mixed distribution is represented as follows:

$$f(y)=\frac{a_1}{\sqrt{2\pi}\delta_1}\exp\left\{-\frac{(y-\mu_1)^2}{2\delta_1^2}\right\}+\frac{a_2}{\sqrt{2\pi}\delta_2}\exp\left\{\frac{(y-\mu_2)^2}{2\delta_2^2}\right\}+\cdots\cdots+\frac{a_n}{\sqrt{2\pi}\delta_n}\exp\left\{-\frac{(y-\mu_n)^2}{2\delta_n^2}\right\} \tag{6}$$

where a_i is the weight; $a_1+a_2+\ldots+a_n=1$; μ_i is the mean; δ_i is the standard deviation.

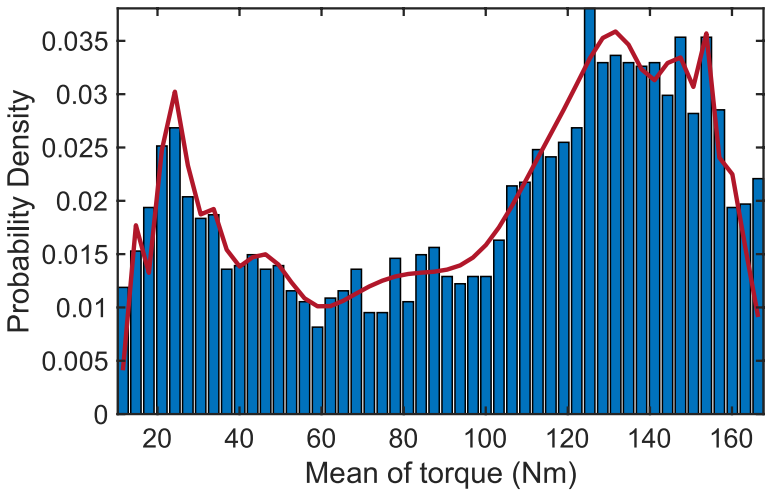

Fig. 12 Gaussian mixed distribution fitting of non-extremum load

Table 4 Sample error calculation values

Mean value μ	Standard deviation σ	Average error value μ_x	Limit error value δ
0.014	0.006	0.062	0.0013

The fitted graph is shown in Fig. 12.

(2) The absolute values of the probability density error between the theoretical fitting curve and the actual load value are calculated, which are used as samples and fitted with normal distribution. The average error values and the limit error values of the probability density error value are calculated with the fitting parameters. The calculation formulas of the average error value and the limit error value are as follows:

$$\mu_x = \frac{\sqrt{\sigma^2/n}}{\mu} \tag{7}$$

where μ_x is the average error value; μ is the mean of normal distribution fitting samples; σ is the standard deviation of normal distribution fitting samples; n is the number of samples.

$$\delta = t \times \mu_x \tag{8}$$

where δ is the limit error value; t is the probability of sampling error, and the sampling limit error is the maximum error, which is 2.1%.

The calculation results are shown in Table 4.

(3) According to the calculated limit error value, the probability density value D_x of the intermediate load x_i fluctuates in the range of $\pm\delta/2$. In this range, the probabil-

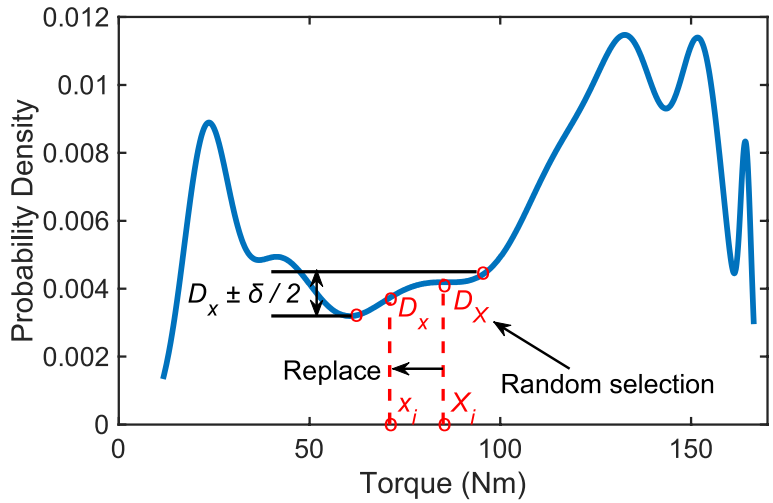

Fig. 13 Intermediate load reproduction process

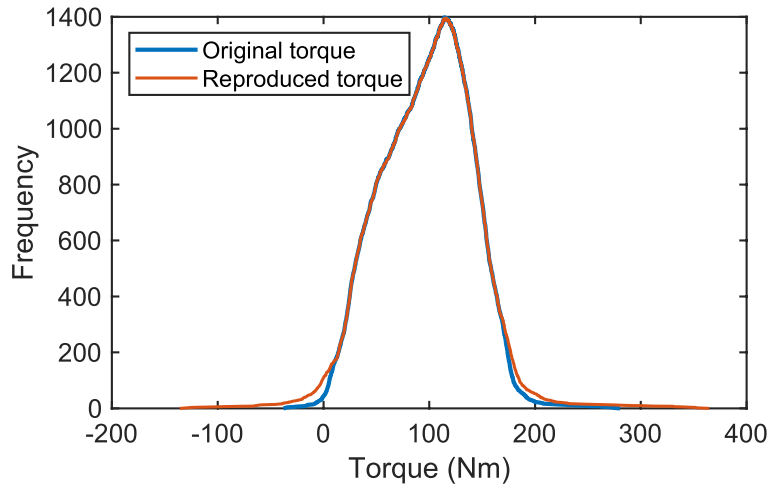

Fig. 14 Comparison of through-level counting before and after load reproduction

ity density value is randomly selected as the probability density value D_X of the new load, and then the new load value X_i is calculated by using the fitted Gaussian mixed probability density function. X_i is the reproduced load. The specific process of reproducing intermediate loads is shown in Fig. 13.

Results and discussion

Comparison of through-level counting

The torque data before and after load reproduction are counted through stages, and the changes of torque data are compared. The comparison of the results of through-level counting is shown in Fig. 14. It can be seen that the data points of the original torque data before the reproduction at the maximum and minimum values are significantly less than those after the reproduction of the extreme value, indicating that the reproduction

of the extreme value expands the data range of the torque, strengthens the user load, and achieves the desired results. The variation trend of the intermediate load after reproduction is highly consistent with the original load, indicating the rationality of the intermediate load reproduction.

Pseudo-damage comparison of ICE

The pseudo-damage is calculated based on the original load before reproduction. The pseudo-damage of the ICE is determined by the rotational speed and torque values. The pseudo-damage calculation method is exhibited as follows:

$$d = \sum_{i=1}^{n} N_i \times \Delta t \times T_i^{\beta} \tag{9}$$

where n is the total number of data points after interpolation of original data; N_i is the speed value; Δt is the time interval between two adjacent data points; T_i is the torque value; β is the damage index, according to engineering experience, β is generally 3 when calculating the pseudo-damage of the ICE.

Combined with Palmgren–Miner linear damage accumulation rule [35], the pseudo-damage value of the ICE before load reproduction is 1.09×10^9, while that after load reproduction is 1.19×10^9. It can be seen that the pseudo-damage value of the torque data before and after reproduction is slightly larger than that of the original data, and the difference is 9.2%. It can be seen that the extreme load and intermediate load are in line with the actual situation before and after reproduction.

Conclusions

In this paper, a time-domain load reproduction method for CMICE based on POT model is proposed. The proposed method provides a reference for the bench test and reliability evaluation of CMICE. The main conclusions of this study are summarized as follows:

1. The outliers of speed and torque are eliminated synchronously when the load of ICE is preprocessed. To ensure the stability of the data, the working conditions are divided based on the average speed data between two adjacent large gradients.
2. The extreme load is reproduced based on POT model and the exceedance mean function graph method is used to select the threshold. The intermediate load is reproduced based on the mixed Gaussian distribution, the probability density error between the actual load and the theoretical distribution is fitted by the normal distribution, and the intermediate load is predicted in the range of the limit error value of the probability density value.
3. The torque load of ICE before and after reproduction is compared by the through-level counting, the relationship between the load level and frequency is counted. The through-level counting curve of the reproduced load and the original load is highly similar. The pseudo-damage of ICE is calculated before and after the reproduction. The pseudo-damage value of ICE under the original load is 1.09×10^9, while the pseudo-damage value after the reproduction is 1.19×10^9. The difference of the

pseudo-damage value before and after the reconstruction is less than 10%, which further illustrates the rationality of the proposed method.

Not only is the CMICE load reproduction method proposed suitable for ICE loads, but also the proposed method in this paper can be used to reproduce the loads in the process of work when evaluating the fatigue life of construction machinery or vehicle parts. The load reproduction method proposed in this paper is a general time-domain load reproduction theory, which can be used as a reference for load reproduction of engineering machinery, vehicles, and aerospace parts.

Abbreviations

CMICE	Construction machinery internal combustion engine
POT	Peak over threshold
ICE	Internal combustion engine
GPD	Generalized Pareto distribution
CAN	Controller Area Network
T_i, T_{i+1}	The moment
N_i, N_{i+1}	Speed value of the corresponding moment
σ	The proportional parameter
ξ	The shape parameter
u	The threshold
a_i	The weight
μ_i	The mean
δ_i	The standard deviation
μ_x	The average error value
μ	The mean of normal distribution fitting samples
σ	The standard deviation of normal distribution fitting samples
n	The number of samples
Δt	The time interval between two adjacent data points
n	The total number of data points after interpolation of original data
β	The damage index

Acknowledgements
Not applicable.

Authors' contributions
Zhijie Li and Yonglai Wang both provided technical guidance and were major contributors in writing the manuscript. Chaoqin Liu analyzed the data and wrote the manuscript draft. Weicheng Kong revised the manuscript and provided the references. Cuicui Chen provided language modification for this article. All authors contributed to the discussion of the results and approved the final manuscript.

Funding
This work was supported by the National Key Laboratory Open Foundation (WCDL-GH-2021-0013).

Availability of data and materials
The datasets generated and analyzed during the current study are not publicly available due to privacy, but are available from the corresponding author on reasonable request.

Declarations

Competing interests
The authors declare that they have no competing interests.

Received: 23 April 2022 Accepted: 27 August 2022
Published online: 01 October 2022

References

1. Men Y, Yu H, Yu H (2017) Development of block loading spectrum for car powertrain rig test correlated with customers' usage. Adv Mech Eng 9:168781401772747. https://doi.org/10.1177/1687814017727472
2. Han Y, Lin Y, Zhang C, Wang D (2021) Customer-related durability test of semi-trailer engine based on failure mode. Eng Fail Anal 120:105095. https://doi.org/10.1016/j.engfailanal.2020.105095

3. Jiménez Espadafor FJ, Becerra Villanueva JA, Palomo Guerrero D, Torres García M, Carvajal Trujillo E, Fernández Vacas F (2014) Measurement and analysis of instantaneous torque and angular velocity variations of a low speed two stroke diesel engine. Mech Syst Signal Process 49:135–153. https://doi.org/10.1016/j.ymssp.2014.04.016
4. Jung D-H, Kim H-J, Pyoun Y-S, Gafurov A, Choi G-C, Ahn J-M (2009) Reliability prediction of the fatigue life of a crankshaft. J Mech Sci Technol 23:1071–1074. https://doi.org/10.1007/s12206-009-0343-2
5. Strozzi A, Baldini A, Giacopini M, Bertocchi E, Mantovani S (2016) A repertoire of failures in connecting rods for internal combustion engines, and indications on traditional and advanced design methods. Eng Fail Anal 60:20–39. https://doi.org/10.1016/j.engfailanal.2015.11.034
6. Fonte M, Reis L, Infante V, Freitas M (2019) Failure analysis of cylinder head studs of a four stroke marine diesel engine. Eng Fail Anal 101:298–308. https://doi.org/10.1016/j.engfailanal.2019.03.026
7. Hermann S, Ruggeri F (2017) Modeling wear in cylinder. Qual Reliab Engng Int 33:839–851. https://doi.org/10.1002/qre.2061
8. Zhiqiang Z, Yongling H, Lifang L, Yang L (2008) Research of plateau compatibility test and evaluation on vehicle engine. In: 2008 IEEE vehicle power and propulsion conference. IEEE, Harbin, pp 1–5
9. Huang F, Lei J, Xin Q (2020) Study on altitude adaptability of a turbocharged off-road diesel engine. J Eng Gas Turbine Power 142:114501. https://doi.org/10.1115/1.4047932
10. Xia M, Zhang F (2020) Application of mul-ti-parameter fuzzy optimization to enhance performance of a regulated two-stage turbocharged diesel engine operating at high altitude. Energies 13:4278. https://doi.org/10.3390/en13174278
11. Wang XC, Hu JB, He X, Guo MC (2013) Pre-diction and analysis of combustion chamber thermal load of heavy vehicle at different altitudes. AMR 706–708:1492–1495. https://doi.org/10.4028/www.scientific.net/AMR.706-708.1492
12. Lee J-H, Jang D-W, Hong S-G, Lee S-B (2017) Evaluating the reliability of the cylinder liner of a low-speed marine engine subjected to high-cycle fatigue with high mean stress. J Mech Sci Technol 31:1639–1644. https://doi.org/10.1007/s12206-017-0311-113
13. Yang W, Pang J, Wang L, Kang X, Zhou S, Zou C, Li S, Zhang Z (2022) Thermo-mechanical fatigue life prediction based on the simulated component of cylinder head. Eng Fail Anal 135:106105. https://doi.org/10.1016/j.engfailanal.2022.106105
14. Rao X, Sheng C, Guo Z, Yuan C (2022) A review of online condition monitoring and maintenance strategy for cylinder liner-piston rings of diesel engines. Mech Syst Signal Process 165:108385. https://doi.org/10.1016/j.ymssp.2021.108385
15. Mohamed ES (2018) Performance analysis and condition monitoring of ICE piston-ring based on combustion and thermal characteristics. Appl Therm Eng 132:824–840. https://doi.org/10.1016/j.applthermaleng.2017.12.111
16. Beranger B, Duong T, Perkins-Kirkpatrick SE, Sisson SA (2017) Exploratory data analysis for moderate extreme values using non-parametric kernel methods. arXiv:160208807 [stat]
17. Xu J, Luo Q, Jing Q, Liu X, Lu J (2019) Research on cyclic time domain extrapolation of diesel engine crankshaft load spectrum based on SVR model. IOP Conf Ser Earth Environ Sci 300:042097. https://doi.org/10.1088/1755-1315/300/4/042097
18. Zheng G, Wang Q, Cai C (2021) Criterion to determine the minimum sample size for load spectrum measurement and statistical extrapolation. Measurement 178:109387. https://doi.org/10.1016/j.measurement.2021.109387
19. Nesterova M, Schmidt F, Soize C (2020) Fatigue analysis of a bridge deck using the peaks-over-threshold approach with application to the Millau viaduct. SN Appl Sci 2:1416. https://doi.org/10.1007/s42452-020-3117-1
20. He J, Zhao X, Li G, Chen C, Yang Z, Hu L, Xinge Z (2019) Time domain load extrapolation method for CNC machine tools based on GRA-POT model. Int J Adv Manuf Technol 103:3799–3812. https://doi.org/10.1007/s00170-019-03774-3
21. Yang X, Liu X, Tong J, Wang Y, Wang X (2018) Research on load spectrum construction of bench test based on automotive proving ground. J Test Eval 46:244–251. https://doi.org/10.1520/JTE20170201
22. Amin NAM, Ismail MS, Hamid HA (2018) Modelling extreme temperature in Perlis using block maxima method. In: Zin SM, Abdullah N, Khazali KAM, Roslan N, Rusdi NA, Saad RM, Yazid NM, Zain NAM (eds) Proceedings of the International Conference on Mathematics, Engineering and Industrial Applications 2018 (ICoMEIA 2018). Amer Inst Physics, Melville, p 020010
23. Ozari C, Eren O, Saygin H (2019) A new methodology for the block maxima approach in selecting the optimal block size. Teh Vjesn 26:1292–1296. https://doi.org/10.17559/TV-20180529125449
24. Dombry C (2015) Existence and consistency of the maximum likelihood estimators for the extreme value index within the block maxima framework. Bernoulli 21:420–436. https://doi.org/10.3150/13-BEJ573
25. An Y, Pandey MD (2005) A comparison of methods of extreme wind speed estimation. J Wind Eng Ind Aerodyn 93:535–545. https://doi.org/10.1016/j.jwei.2005.05.003
26. Harris RI (2001) The accuracy of design values predicted from extreme value analysis. J Wind Eng Ind Aerodyn 89:153–164. https://doi.org/10.1016/S0167-6105(00)00060-X
27. Wang Q, Zhou J, Gong D, Wang T, Sun Y (2021) Fatigue life assessment method of bogie frame with time-domain extrapolation for dynamic stress based on extreme value theory. Mech Syst Signal Process 159:107829. https://doi.org/10.1016/j.ymssp.2021.107829
28. Liang B, Shao Z, Li H, Shao M, Lee D (2019) An automated threshold selection method based on the characteristic of extrapolated significant wave heights. Coast Eng 144:22–32. https://doi.org/10.1016/j.coastaleng.2018.12.001
29. Jixin W, Yan W, Xinting Z, Yajun H, Zhenyu W (2018) Automatic determination method of optimal threshold based on the bootstrapping technology. J Southeast Univ 34(2):208–212
30. Wang J, Zhai X, Liu C, Zhang Y (2017) Determination of the threshold for extreme load extrapolation based on multi-criteria decision-making technology. SV-JME 63:201–211. https://doi.org/10.5545/sv-jme.2016.3557

31. Yang Z, Song Z, Zhao X, Zhou X (2021) Time-domain extrapolation method for tractor drive shaft loads in stationary operating conditions. Biosyst Eng 210:143–155. https://doi.org/10.1016/j.biosystemseng.2021.08.020
32. Liu X, Zhang M, Wang H, Luo J, Tong J, Wang X (2020) Fatigue life analysis of automotive key parts based on improved peak-over-threshold method. Fatigue Fract Eng Mater Struct 43:1824–1836. https://doi.org/10.1111/ffe.13235
33. Wang H, Xuan F, Liu X (2021) Prediction and evaluation of fatigue life under random load based on low load strengthening characteristic. Int J Fatigue 151:106346. https://doi.org/10.1016/j.ijfatigue.2021.106346
34. Schwertman NC, Owens MA, Adnan R (2004) A simple more general boxplot method for identifying outliers. Comput Stat Data Anal 47:165–174. https://doi.org/10.1016/j.csda.2003.10.012
35. Post N, Case S, Lesko J (2008) Modeling the variable amplitude fatigue of composite materials: a review and evaluation of the state of the art for spectrum loading. Int J Fatigue 30:2064–2086. https://doi.org/10.1016/j.ijfatigue.2008.07.002

Publisher's Note